AD NUMBER

AD528775

LIMITATION CHANGES

TO:

Approved for public release; distribution is unlimited.

FROM:

**Distribution authorized to U.S. Gov't. agencies and their contractors;
Administrative/Operational Use; JAN 1974. Other requests shall be referred to Defense Advanced Research Projects Agency, Washington, DC 20301.**

AUTHORITY

darpa ltr dtd 26 Oct 1983

AD NUMBER
AD528775
CLASSIFICATION CHANGES
TO: **UNCLASSIFIED**
FROM: **SECRET**
AUTHORITY
26 Oct 1983, per darpa ltr

AD- 528775

SECURITY REMARKING REQUIREMENTS

DOD 5200.1-R, DEC 78

REVIEW ON 18 JAN 94

ESD-TR-74-13

Secret

Technical Note 1974-6

J. O. Dimmock

Sensor Capabilities

(Title UNCLASSIFIED)

18 January 1974

Prepared for the Advanced Research Projects Agency
under Electronic Systems Division Contract F19628-73-C-0002 by

Lincoln Laboratory
MASSACHUSETTS INSTITUTE OF TECHNOLOGY
LEXINGTON, MASSACHUSETTS

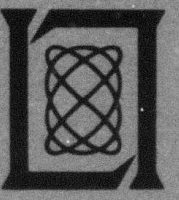

Secret

Secret

This document comprises 40 pages. No. 23 of 60 copies.

MASSACHUSETTS INSTITUTE OF TECHNOLOGY

LINCOLN LABORATORY

SENSOR CAPABILITIES

(Title UNCLASSIFIED)

J. O. DIMMOCK

Group 52

TECHNICAL NOTE 1974-6

18 JANUARY 1974

LEXINGTON MASSACHUSETTS

Secret

The work reported in this document was performed at Lincoln Laboratory, a center for research operated by Massachusetts Institute of Technology. This work was sponsored by the Advanced Research Projects Agency of the Department of Defense under Air Force Contract F19628-73-C-0002 (ARPA Order 600).

ABSTRACT

(U) This note describes the detailed calculations and considerations necessary to estimate infrared exoatmospheric sensor capabilities. Two types of sensors are compared, an infrared vidicon type image tube and a scanned linear array. Although both systems appear capable of high-altitude satellite surveillance, the required optics diameter for the vidicon system is significantly less than for the linear array.

Accepted for the Air Force
Eugene C. Raabe, Lt. Col., USAF
Chief, ESD Lincoln Laboratory Project Office

J.O. Dimmock

SENSOR CAPABILITIES

I. RANGE EQUATION

[U] In general, the sensor can be considered to consist of a collection and focusing optics system (telescope), a detector system, which may consist of a linear array of individual elements, a vidicon or possibly other types of LWIR sensitive units which convert the infrared signal into an electrical signal, and an electronic system which converts this electrical signal into usable information.

A. Linear Array

[U] The radiant flux per unit area $H_{\Delta\lambda}$ available to the sensor in its operating spectral bandwidth, $\Delta\lambda$, is related to the target radiance in this wavelength region, $W_{\Delta\lambda}$; the projected area of the target, A; and the sensor-to-target range, R, by

$$H_{\Delta\lambda} = \frac{W_{\Delta\lambda} A}{\pi R^2} \quad (W/cm^2) \quad . \tag{A-1}$$

$W_{\Delta\lambda}$ is related to the target temperature, effective emissivity-area product and spectral band of the sensor. The target spectral radiance, W_{λ}, is shown in Fig. A-1 as a function of wavelength for various target temperatures. The scale is for a black body target of unit emissivity. Grey body targets with emissivities less than one would produce correspondingly less irradiance.

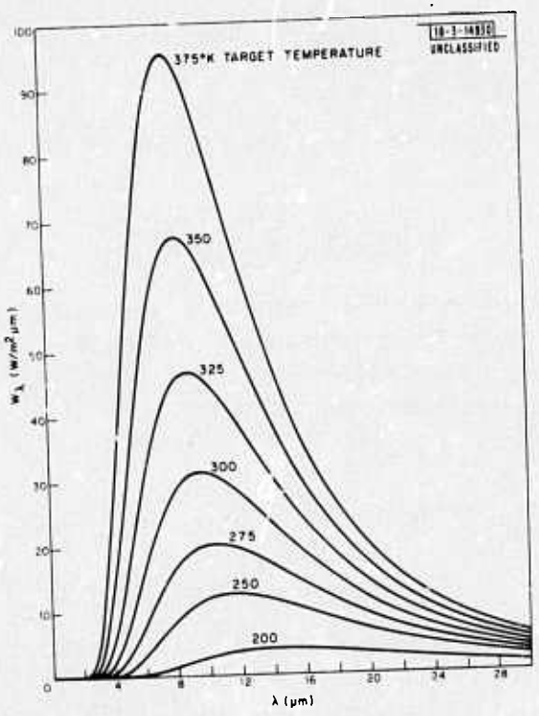

Fig. A-1. Target irradiance vs wavelength for blackbody targets of various temperatures. [U]

Figure A-1 indicates that the spectral range of principal interest for a 300°K target is between about 6 and 18 μm and also that the total radiance is a strong function of the target temperature.

[U] Nominal target and range considerations define the minimum value of $H_{\Delta\lambda}$ which the sensor must be capable of detecting. Given a required system signal-to-noise ratio (SNR) this determines the required sensor noise-equivalent-flux-density (NEFD)

$$(NEFD)_{required} = \min (H_{\Delta\lambda})/(SNR) \qquad (W/cm^2) \quad . \tag{A-2}$$

[U] The NEFD of the sensor determines to a large degree its capabilities for detecting and obtaining orbital parameters of nominal space objects. The NEFD can in turn be related to the detector and telescope characteristics by

$$NEFD = \frac{NEP}{A_o T_o} B^{1/2} \qquad (W/cm^2) \tag{A-3}$$

where NEP refers to the detector-amplifier noise-equivalent-power per unit electrical bandwidth, A_o is the primary collection optics area, T_o is the transmission efficiency of the telescope and B is the electrical bandwidth. In a scanned linear array system the optimum value of B is related to the dwell time τ of the target image on a detector approximately by

$$B = 1/2\tau \quad . \tag{A-4}$$

As an alternative to the NEP, the detector sensitivity is frequently expressed in terms of D* (dee-star) which is defined as

$$D^* = \frac{A_d^{1/2}}{NEP} \qquad (cmHz^{1/2}/W) \tag{A-5}$$

where A_d is the detector area.

[U] Combining Eqs. (A-1) through (A-4), we obtain a range-capability equation for a linear array

$$R^2 = \frac{W_{\Delta\lambda} A}{\pi (SNR)} \frac{A_o T_o}{NEP} (2\tau)^{1/2} \quad . \tag{A-6}$$

In a search scheme we are interested in how rapidly a given region of space can be searched with the required range-sensitivity. The search rate $\dot{\Omega}$ is related to the required dwell time, τ, the instantaneous field-of-view (ω_{FOV}) of the individual detectors in the array and the number of detectors in the array, n, by

$$\dot{\Omega} = n\omega_{FOV}/\tau \tag{A-7}$$

so that Eq. (A-6) becomes

$$R^2 = \frac{W_{\Delta\lambda} A}{\pi (SNR)} \frac{A_o T_o}{NEP} (2n\omega_{FOV})^{1/2} \dot{\Omega}^{-1/2} \tag{A-8a}$$

or alternatively in terms of D*

$$R^2 = \frac{W_{\Delta\lambda} A}{\pi (SNR)} A_o T_o D^* \left(\frac{2n\omega_{FOV}}{A_d}\right)^{1/2} \dot{\Omega}^{-1/2} \tag{A-8b}$$

[U] The instantaneous field-of-view, ω_{FOV}, is given by

$$\omega_{FOV} = \frac{A_d}{F^2} \tag{A-9}$$

where F is the focal length of the optical system. Equations (A-8) and (A-9) can be combined to give

$$R^2 = \frac{W_{\Delta\lambda} A}{4(SNR)} \frac{DT_o}{f \cdot NEP} (2nA_d)^{1/2} \dot{\Omega}^{-1/2} \tag{A-10a}$$

or

$$R^2 = \frac{W_{\Delta\lambda} A}{4(SNR)} \frac{DT_o}{f} D^* (2n)^{1/2} \dot{\Omega}^{-1/2} \tag{A-10b}$$

where $A_o = (\pi/4) D^2$, D is the collection optics diameter and f = F/D is the f-number of the optical system. If the NEP is independent of the detector area, as is the case for amplifier noise limited operation, Eq. (A-10a) indicates that the range-scan rate can be increased by increasing the detector area, thus increasing ω_{FOV}. There is a limit to this, however, imposed by the point source stellar background. If ρ is the density of stars with flux greater than the detection threshold of the system then at any instant the probability that a given detector will be obscured by a star in its field-of-view is

$$\epsilon = \rho \omega_{FOV} \tag{A-11}$$

If we demand that ϵ be less than a given value the star density ρ sets an upper limit on ω_{FOV}. The stellar density ρ depends on the direction of observation relative to the galactic plane, the spectral bandwidth of the sensor and, of course, the NEFD or system range requirements. It also turns out in practice that as the detectors are made larger the NEP will eventually increase as $A_d^{1/2}$ making D* independent of detector area. This occurs, for example, when the detectors become background limited. In this situation the range sensitivity is independent of the instantaneous individual detector field-of-view. In addition there may be an advantage in some cases of reducing the size of the detectors in order to increase the tracking accuracy.

B. Vidicon

[U] The range sensitivity of a vidicon can be expressed in a manner formally equivalent to that of the linear array. Replacing Eq. (A-6) we have

$$R^2 = \frac{W_{\Delta\lambda} A}{\pi(SNR)} \frac{A_o T_o}{NEP} (2t_F)^{1/2} \tag{A-12}$$

where t_F is the frame time of the vidicon and NEP is the noise-equivalent-power of a minimum resolution element. In the case of the vidicon

$$\dot{\Omega} = \Omega_{FOV}/t_F \tag{A-13}$$

where Ω_{FOV} is the vidicon-sensor instantaneous field-of-view. Equation A-12 becomes

$$R^2 = \frac{W_{\Delta\lambda} A}{\pi(SNR)} \frac{A_o T_o}{NEP} (2\Omega_{FOV})^{1/2} \dot{\Omega}^{-1/2} \tag{A-14}$$

or using $\Omega_{FOV} = A_r/F^2$ where A_r is the area of the vidicon retina

$$R^2 = \frac{W_{\Delta\lambda} A}{4(SNR)} \frac{DT_o}{NEP} \frac{(2A_r)^{1/2}}{f} \dot{\Omega}^{-1/2} \quad . \tag{A-15}$$

As in the case with the linear array we would like a low f-number system. The other driving factors are the area of the vidicon retina and the NEP.

II. LINEAR ARRAY CAPABILITIES

A. Fundamental Detector Limitations

[U] In this section we consider the fundamental limitations to the sensitivity of individual extrinsic LWIR detectors.[A-1,A-2] Keyes and Quist[A-2] have considered five dominant noise sources in their characterization of an extrinsic (impurity doped) photoconductor. The signal current is given by

$$i_s = \frac{q\eta G P_s}{h\nu} \tag{A-16}$$

where q is the electron charge, η and G are the detector quantum efficiency and gain, respectively, P_s is the signal power and $h\nu$ is the signal photon energy. The noise current can be written as

$$i_n = \left(4qi_t G + \frac{4kT_d}{R_d} + \frac{4kT_L}{R_L}\right)^{1/2} \cdot B^{1/2} \tag{A-17}$$

where i_t is the total current generated in the detector, T_d and R_d are the detector temperature and resistance, respectively, T_L and R_L are the load resistor temperature and resistance, respectively, and B is the bandwidth. The last two terms in Eq. (A-17) represent the Johnson noise in the detector and in the amplifier circuit. The first term represents the generation-recombination noise and is a sum of three contributions.

$$i_t = i_s + i_b + i_T \tag{A-18}$$

where i_s is the signal current given by Eq. (A-16), i_b is the current due to the background and is given by

$$i_b = \frac{q\eta G P_b}{h\nu} \tag{A-19}$$

where P_b is the non-equilibrium background power falling on the detector, and i_T is the thermal generation-recombination current within the detector. This can be written for acceptor impurity photoconductors as[A-2]

$$i_T = \frac{2qG}{g\tau_p} \frac{N_A - N_D}{N_D} A_d w \left(\frac{2\pi m^* kT_d}{h^2}\right)^{3/2} \cdot \exp\left[-\frac{E_i}{kT_d}\right] \quad \text{(A-20)}$$

where

g = the effective degeneracy of the impurity ground state

τ_p = the hole (majority carrier) lifetime

N_A = the acceptor concentration

N_D = the donor concentration

A_d = the detector area

w = the detector thickness

m^* = the hole (majority carrier) mass

T_d = the detector temperature

k = Boltzman's constant

h = Planck's constant

E_i = the impurity ionization energy

(The roles of N_A and N_D are reversed for donor impurity photoconductors.)

[U] The lifetime of the photoexcited carriers can be written as

$$\tau_p = \frac{1}{B_r N_D} \quad \text{(A-21)}$$

where B_r is the recombination coefficient. Also there will be a relationship between $(N_A - N_D)$ and the quantum efficiency given by

$$\eta = \frac{(1 - r)\{1 - \exp[-\sigma_A (N_A - N_D) w]\}}{1 - r \exp[-\sigma_A (N_A - N_D) w]} \quad . \quad \text{(A-22)}$$

where r is the reflectivity of the detector material and σ_A is cross section for infrared absorption by the $N_A - N_D$ acceptors available for excitation. Given r, η defines a unique value for the quantity

$$a(\eta) = \sigma_A \frac{(N_A - N_D) w}{\eta} \quad . \quad \text{(A-23)}$$

Substituting Eqs. (A-21) and (A-23) into Eq. (A-20) we obtain

$$i_T = 2qGB_r \frac{a(\eta)\,\eta}{\sigma_A g} A_d \left(\frac{2\pi m^* kT_d}{h^2}\right)^{3/2} \exp\left[-\frac{E_i}{kT_d}\right] \quad . \quad \text{(A-24)}$$

[U] Before collecting terms it is useful to re-express the background power in terms of the background photon flux density Q_b in photons/sec cm^2

$$P_b = h\nu Q_b A_d \tag{A-25}$$

so that Eq. (A-19) becomes

$$i_b = q\eta G Q_b A_d \quad . \tag{A-26}$$

The detector NEP, per unit bandwidth, the way we have defined it above is given by

$$NEP = \frac{i_n}{i_s} P_s B^{-1/2} \quad . \tag{A-27}$$

Using this and Eq. (A-5) we obtain for the detectivity

$$D^*_\lambda = \frac{\eta^{1/2}}{2h\nu}\left\{\frac{P_s}{h\nu A_d} + Q_b + \frac{k}{q^2 G^2 \eta A_d}\left(\frac{T_d}{R_d} + \frac{T_L}{R_L}\right) + 2\,\frac{a(\eta)}{\sigma_A g} B_r \left(\frac{2\pi m^* k T_d}{h^2}\right)^{3/2} \exp\left[-\frac{E_i}{kT_d}\right]\right\}^{-1/2} \quad . \tag{A-28}$$

which corresponds to Eq. (A-22) of Keyes and Quist. Equation (A-28) does not include any noise contribution from the amplifier. The amplifier limited detectivity can be written in the form

$$[D^*_\lambda]_{\text{amplifier}} = \frac{q\eta G}{h\nu} A_d^{1/2} R_L / V_N(f) \tag{A-29}$$

where $V_N(f)$ is the frequency dependent amplifier noise voltage to take two phenomena into account. First there is usually an $R_L C$ roll-off in the signal characteristic of the load resistor – stray capacitance time constant. The signal current should thus be multiplied by $(1 + \omega^2 R_L^2 C^2)^{-1/2}$ where $f = 2\pi\omega$ is the center frequency of the electrical measurement. This roll-off factor does not affect the other terms in Eq. (A-28) since the noise current coming from the detector rolls off in the same manner. The noise from the amplifier, however, in general does not. The second factor is the frequency dependence of the amplifier noise. This is generally taken into account by directly including a frequency dependent amplifier noise voltage, $V_N(f)$, so that Eq. (A-29) becomes

$$[D^*_\lambda]_{\text{amplifier}} = \frac{q\eta G A_d^{1/2} R_L}{h\nu V_N(f)\,(1 + \omega^2 R_L^2 C^2)^{1/2}} \tag{A-30}$$

Thus Eq. (A-28) should be replaced by

$$D^*_\lambda = \frac{\eta^{1/2}}{2h\nu}\left\{\frac{P_s}{h\nu A_d} + Q_b + \frac{1}{4q^2\eta G^2 A_d}\left[\frac{4kT_d}{R_d} + \frac{4kT_L}{R_L} + \frac{V_N^2(1 + \omega^2 R_L^2 C^2)}{R_L^2}\right] + 2\,\frac{a(\eta)}{\sigma_A g} B_r \left(\frac{2\pi m^* k T_d}{h^2}\right)^{3/2} \exp\left[-\frac{E_i}{kT_d}\right]\right\}^{-1/2} \quad . \tag{A-31}$$

In the remainder of this section we consider the effect of the various terms in Eq. (A-31) on the detectivity.

1. Signal Noise Limit

[U] It is easy to show that the signal noise limited NEP is given by

$$NEP_s = 4h\nu B^{1/2}/\eta \quad . \qquad (A-32)$$

If we relate $B = 1/2\tau$ this effectively says that for $\eta = 1$ we can detect two photons in a given time interval with SNR = 1 in the signal noise limited region. In terms of the NEP for a wavelength of 10 μm and $\eta = 0.5$, $NEP_s = 1.6 \times 10^{-19} B^{1/2}$ $(W/Hz^{1/2})$. This will not turn out to be a limiting factor as we shall see that both the background and amplifier limits are higher.

2. Background Limit

[U] The background photon flux density originates from two major sources, celestial background and the telescope cavity thermal background.

[U] Celestial Backgrounds:- The celestial background experienced by an LWIR exo-atmospheric sensor has been discussed at some length by Garing, Stair, and Walker.[A-3] They divide their discussion into two parts; the first concerns stellar objects having a spatial extent small compared to the field-of-view of a single detector element. As indicated above, the star density effectively limits the angular field-of-view which each detector can be allowed to subtend and still not have a high probability of being obscured by a bright object. Considerable data on the stellar population density as a function of radiant intensity has been accumulated in recent sounding rocket observations using sensitive LWIR detectors. These data are in the process of being analyzed and should give an indication of the densities to be expected. Unfortunately they cover a relatively high-intensity flux range and must be extrapolated several orders-of-magnitude to the flux density range of interest here. This is discussed in more detail in Appendix B.

[U] The second part of Garing, Stair and Walker's discussion covered the problem of diffuse backgrounds. These consist principally of zodiacal emission, galactic emission and the cosmic background.

[U] The zodiacal emission is concentrated in the plane of the solar system and apparently consists primarily of thermal radiation from dust grains heated by solar radiation. Some measurements of the zodiacal emission have been made recently by Soifer, Houck and Harwit[A-4] using a sounding rocket equipped with sensors covering the 5-6, 12-14, 16-23 and 70-130 μm regions. Plots of their results for the 12-14 and 16-23 μm regions are shown in Fig. A-2. A quasi-theoretical fit to the 12-14 μm data generated by us is included and discussed below. A summary of their observations is given in Table A-1. Their measurements were made at an elongation of 160° and their measured intensity appears to be peaked within ±10° of the ecliptic plane. At angles greater than this the radiation appears to be about $1 - 2 \times 10^{-11}$ W/cm^2 μm sr which forms an upper limit for the uniform cosmic background.

[U] An attempt can be made to obtain an estimate of the zodiacal emission at angles from the ecliptic plane greater than the ±10° range covered by the measurements of Soifer, Houck and Harwit. If the emission is assumed to originate from a disk of half angle Θ_o then the flux for

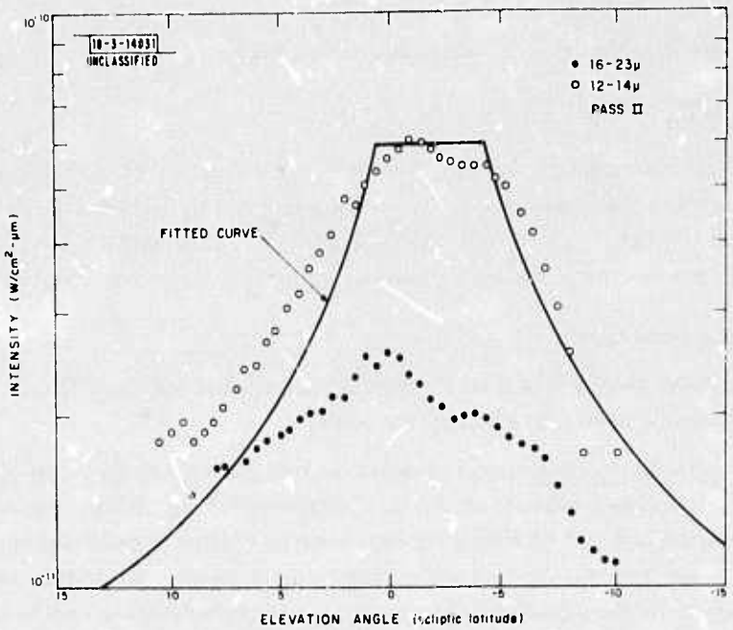

Fig. A-2. Zodiacal radiation intensity as a function of ecliptic angle for 12-14 μm and 16-23 μm detectors. [U]

TABLE A-1† [U]

OBSERVED FLUXES [U]

Detector	λ(μm)	Noise Equivalent Intensity‡	Minimum Detected Intensity‡	Minimum Signal‡ – Scattered Earthlight	Ecliptic Flux‡ Upper Limit (pass 1)	Ecliptic Flux‡ Upper Limit (pass 2)
Ge:Cu	5-6	1.3×10^{-13}	3×10^{-11}	2×10^{-11}	$< 6.5 \times 10^{-11}$	$3. \times 10^{-11}$
Ge:Cu	12-14	8×10^{-14}	3×10^{-11}	2×10^{-11}	$< 7.0 \times 10^{-11}$	6.0×10^{-11}
Ge:Cu	16-23	2.3×10^{-14}	1.8×10^{-11}	1.2×10^{-11}	$< 4 \times 10^{-11}$	2.5×10^{-11}
Ge:Ga	70-130	6×10^{-14}	1.4×10^{-12}	1.0×10^{-12}	$< 1.4 \times 10^{-12}$	$< 9 \times 10^{-12}$

† Based on data of Soifer, Houck and Harwit.

‡ Intensity in units of watts $(cm^2\ sr\ \mu m)^{-1}$.

elevation angle $\Theta \leq \Theta_o$ is W_o, independent of Θ whereas for $\Theta > \Theta_o$ the flux is given by

$$W(\Theta) = W_o \frac{\sin\Theta_o}{\sin\Theta}$$

this function is plotted in Fig. A-2 along with the data. The fit is established at $\Theta_o = \pm 2.5°$ off the center of the major flux region which for the 12-14 μm radiation appears to be shifted off the ecliptic plane by −2°. An extension of this theoretical curve to larger elevation angles is shown

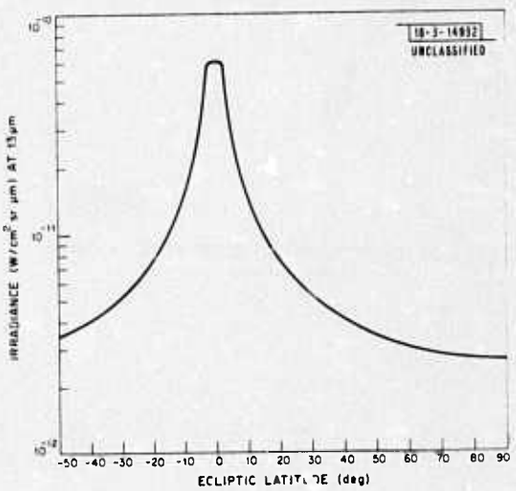

Fig. A-3. Theoretical extrapolation of the zodiacal irradiance measured by Soifer, Houck and Harwit (Ref. A-4). [U]

in Fig. A-3. This model can be used to calculate the zodiacal infrared background limited detectivity as a function of angle off the ecliptic plane. The background limited detectivity can be obtained from Eq. (A-31) using

$$Q_b = \frac{T_o Q_B}{4f^2} \tag{A-33}$$

where Q_B is the background photon flux (photons/sec cm^2) at the entrance aperture. This gives a background limited detectivity of

$$D^*_\lambda = \frac{f}{h\nu}\left(\frac{\eta}{T_o Q_B}\right)^{1/2} . \tag{A-34}$$

The resultant zodiacal radiation limited detectivity is shown in Fig. A-4 vs ecliptic latitude using the irradiance curves of Fig. A-3, $\eta = 0.5$, $T_o = 0.5$, $f = 1.5$ and $\lambda = 14$ μm for a detector spectral bandwidth of 8-14 μm. Estimates of the cosmic background limits are also shown. The curves are approximately correct for detectors covering the wavelength region between 8 and 14-22 μm. The detectivity values should be reduced by about 8 percent if the 6-14 μm region were covered.

[U] The cosmic background forms perhaps the most fundamental limit to the sensitivity of exoatmospheric sensors. Unfortunately no measurements of this radiation have been reported and its theoretical magnitude depends strongly on which model one assumes for the space-time characteristics of the universe. Figure A-5 shows the cosmic background radiance calculated

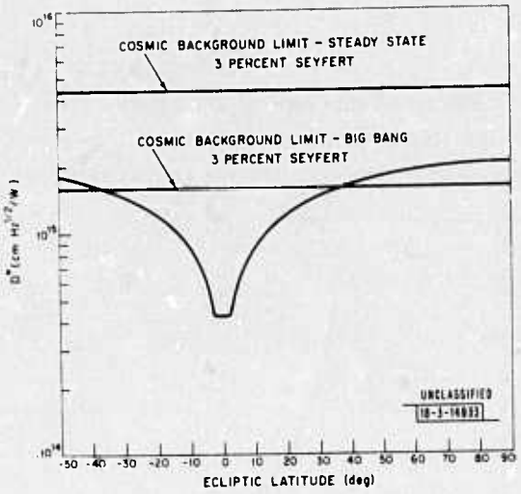

Fig. A-4. Zodiacal irradiance and cosmic background limited detectivity, D*, vs ecliptic latitude. The curves are calculated for $\eta = 0.5$, $T_o = 0.5$, $f = 1.5$, and $\lambda = 14\,\mu m$ for a spectral band of 8-14 μm. [U]

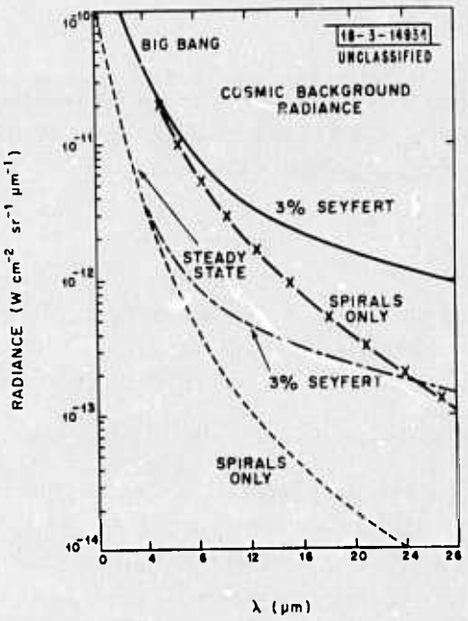

Fig. A-5. The cosmic background radiance derived for both the Steady-State and Evolutionary, or "Big Bang," models of the universe. The cross-hatched curve is for a Big Bang model universe filled with spiral galaxies only, while the solid curve is the same model, but with the universe filled with 97 percent spiral galaxies and 3 percent Seyfert galaxies. Similar remarks apply to the dashed and dot-dashed curves for the steady-state model. [U]

using the "steady state" and "big bang" models of the universe.[A-3] One observes as much as two orders of magnitude difference between the various models. Approximate upper limits to the achievable detectivity, however, can be obtained using these theoretical results. These limits are only slightly higher than those imposed by the zodiacal radiation and the limits assuming 3 percent Seyfert galaxies are included for comparison in Fig. A-5.

[U] Telescope Background:– The thermal emission flux from the telescope walls is given by

$$Q_b = 2\pi c\alpha \int \frac{d\lambda}{\lambda^4 [\exp(hc/\lambda kT) - 1]} \quad \text{(photons/sec cm}^2\text{)} \qquad \text{(A-35)}$$

where T is the effective telescope temperature. The integral is taken over the spectral bandwidth of the detector and $\alpha \leq 1$ is introduced to take account of the fact that the telescope walls subtend somewhat less than a 2π field-of-view from the detector plane. In Fig. A-6 we plot the telescope background limited detectivity assuming $\eta = 1$, $\alpha = 1$ vs telescope temperature for various long wavelength detector limits. Note that the curves remain unchanged for $\alpha = \sqrt{\eta}$, for example $\alpha = 0.7$, $\eta = 0.5$ which is a reasonable combination of parameters. In Fig. A-7 we plot the background limited detectivity vs the detector long wavelength limit for various background temperatures.

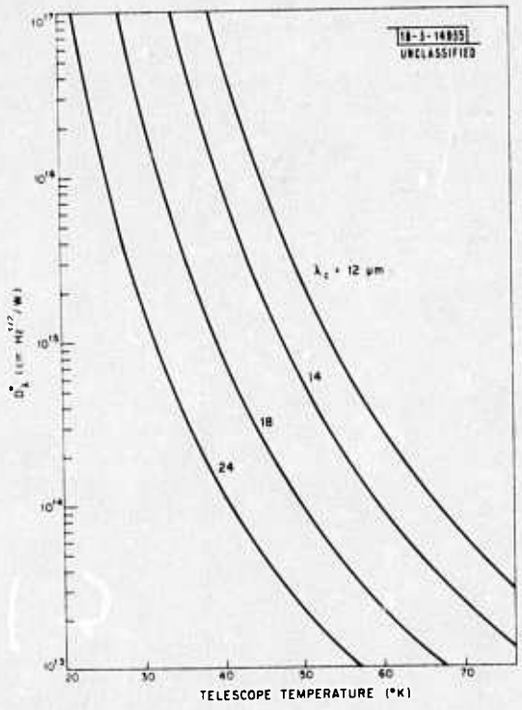

Fig. A-6. Telescope background limited detectivity vs telescope temperature. [U]

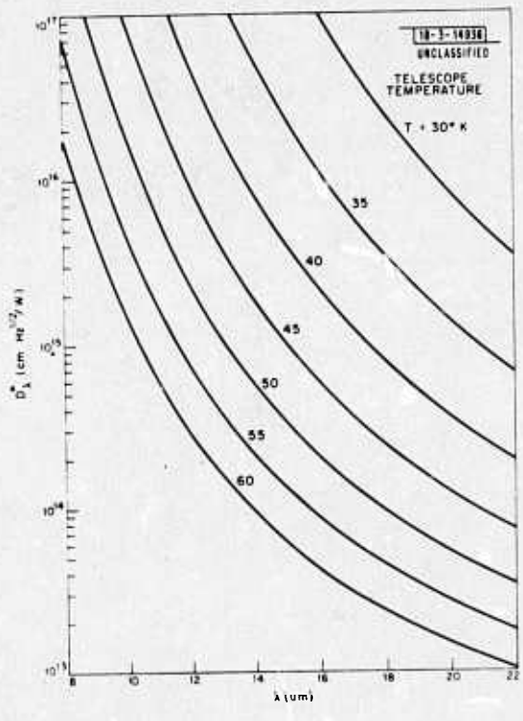

Fig. A-7. Telescope background limited detectivity vs detector long wavelength cutoff limit. [U]

TABLE A-2 [U]

PROPERTIES OF EXTRINSIC SILICON DETECTORS [U]

Type	E_i (eV)	λ_{pk} (μm)	$\lambda_{1/2}$ (μm)	$\sigma_A(\lambda_{pk})$ (10^{-15} cm^2)	m^*/m_o	g
Si:B (p)	0.045	23.5	28.5	1.8	0.59	4
Si:Al (p)	0.057	15	18.2	0.85	0.59	4
Si:Ga (p)	0.065	14.5	17.5	0.56	0.59	4
Si:In (p)	0.16	5.2	8.6	0.21	0.59	4
Si:Sb (n)	0.039	28.8	31	7.2	1.08	2
Si:P (n)	0.044	27.0	30.0	2.2	1.08	2
Si:As (n)	0.055	22.5-23	24.0-24.5	1.5	1.08	2
Si:Bi (n)	0.069	16.5	18.7	0.7	1.08	2

Silicon

η	$a(\eta)$
0.50	2.10
0.40	1.69
0.30	1.43
0.25	1.34
0.20	1.25
0.15	1.20
0.10	1.10
0.05	1.04
0.025	1.00

3. Detector Noise Limit

[U] The detector generation-recombination (g-r) noise limited detectivity is given by the last term in Eq. (A-31), namely

$$D^*_\lambda = \frac{\eta^{1/2}}{2h\nu}\left\{2\,\frac{a(\eta)}{\sigma_A g}\,B_r\left(\frac{2\pi m^* kT_d}{h^2}\right)^{3/2}\exp\left[-\frac{E_i}{kT_d}\right]\right\}^{-1/2} \quad . \tag{A-36}$$

The approximate values for the various parameters contained in Eq. (A-36) are given in Table A-2 for extrinsic doped silicon detector materials.[A-5] In Fig. A-8, we plot D^*_λ peak against detector temperature, T_d, for the various detector types using the parameters given in Table A-2 and

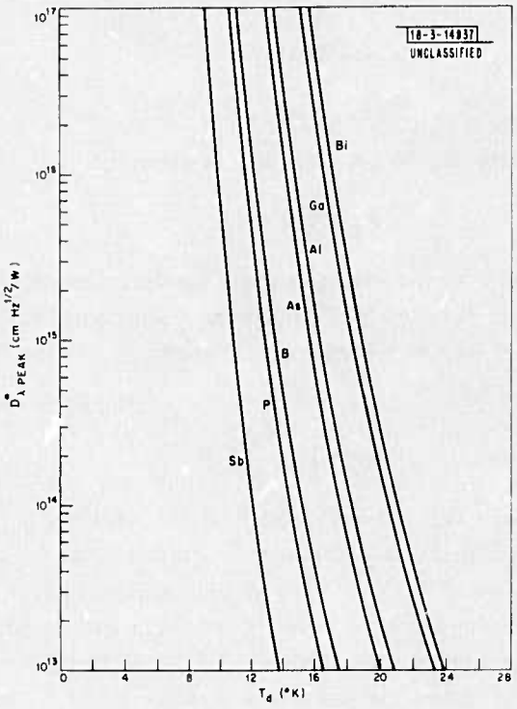

Fig. A-8. Detector g-r noise limited D^*_λ vs detector temperature for various extrinsic photoconductive silicon detectors. The curve labels indicate the impurity used. [U]

$\eta = 0.5$, $a(\eta) = 2.10$. There is a large uncertainty in the recombination coefficient B quoted in the literature as pointed out by Sclar. In Fig. A-8 we have used a value of 3×10^{-6} cm^3 sec^{-1} as being a rough average of those values indicated by Sclar.[A-5] According to Sclar this should be approximately independent of impurity species. In Table A-3 we give the detector temperature necessary to achieve a D^*_λ, peak of 10^{15} cmHz$^{1/2}$/W which corresponds to the zodiacal radiation limited value for an ecliptic elevation angle of about ±15° at an elongation of 160°. Also given in the table are the approximate telescope temperatures necessary to achieve this detectivity for the peak wavelengths of the various detectors.

[U] It can be shown that the detector Johnson noise given by the second term in Eq. (A-17), is, in general, negligible compared to the generation-recombination noise given by the first term.

TABLE A-3 [S]

DETECTOR AND TELESCOPE TEMPERATURES NECESSARY TO ACHIEVE D^*_{λ}, peak = 10^{15} cmHz$^{1/2}$/W FOR VARIOUS EXTRINSIC Si DETECTORS [U]

Type	λ_{peak} (μm)	T_{det} (°K)	T_{optics} (°K)
Si:B	23.5	13.5	32
Si:Al	15	16.3	45
Si:Ga	14.5	18.3	46
Si:Sb	28.8	10.8	27
Si:P	27.0	12.8	29
Si:As	22.5	15.7	33
Si:Bi	16.5	19.0	42

The detector resistance, R_d, is given by

$$R_d = V/I = V/i_t \qquad \text{(A-37)}$$

where V is the voltage across the detector and $I = i_t$ is the total current passing through the detector. It is generally found experimentally that there is no measurable additional (leakage) current beyond the generated current i_t. Using Eq. (A-37) in Eq. (A-17) we can regroup the first two terms as

$$4qi_tG\left(1 + \frac{kT_d}{qGV}\right) .$$

Optimum values of the bias field for extrinsic doped Si detectors are found to be about 100 V/cm. The minimum detector element size is given by 2.44 fλ, the diffraction limit for the optical system. For f = 1.5, λ = 1.4 μm this dimension is 51 μm = 2 mils. Consequently the smallest value of V to be expected under normal operating conditions is about 0.5 V. The highest detector operating temperature given in Table A-3 is 19°K. Using 20°K for T_d and 0.5 V, $kT/qV = 3.4 \times 10^{-3}$. Typical values for the detector gain are G = 0.2 to 0.5. Using G = 0.2, kTd/qGV = 0.017 so that this term gives at most a 2 percent contribution in the worst case.

4. Amplifier Limit

[U] The amplifier noise limited detectivity was given by Eq. (A-30) and is repeated here

$$[D^*_{\lambda}]_{amplifier} = \frac{q\eta G A_d^{1/2} R_L}{h\nu V_N(f)\,(1 + \omega^2 R_L^2 C^2)} .$$

Typical values of the load resistor, R_L, range from 10^{10} to 10^{11} ohms and parasitic capacitance values are of the order of 8 pF so that R_LC is like 0.08 to 0.8 sec and $2\pi R_LC$ is like 0.5 to 5 sec. Since typical measurement frequencies are greater than a few Hz, $\omega R_LC = 2\pi f R_LC$ is generally large so that Eq. (A-30) can be approximated by

$$[D^*_\lambda]_{\text{amplifier}} \simeq \frac{q\eta G A_d^{1/2}}{h\nu\, V_N(f)\, 2\pi f C} \quad . \tag{A-38}$$

This can again be rewritten in terms of the detector responsivity, R_a(amps/watt) = $q\eta G/h\nu$, as

$$[D^*_\lambda]_{\text{amplifier}} \simeq \frac{R_a A_d^{1/2}}{V_N(f)\, 2\pi f C} \quad . \tag{A-39}$$

Responsivity values as high as 10 A/W have been observed for Si:As detectors at 19 μm by Sclar. This corresponds to an ηG product of 0.65. This most likely reflects a gain of near unity and a quantum efficiency somewhat over 50 percent.

[U] It is generally found that the amplifier noise voltage $V_N(f)$ (volts/$Hz^{1/2}$) varies approximately as $f^{-1/2}$ with typical values at f = 5 Hz of $\sim 6 \times 10^{-7}$ V/$Hz^{1/2}$. We can define a new quantity

$$\overline{V}_N = V_N(f)\, f^{1/2} \qquad \text{(volts)} \quad . \tag{A-40}$$

Since $[D^*_\lambda]_{\text{amplifier}}$ given by Eq. (A-39) is detector area dependent it is perhaps more useful to refer to the detector NEP which would be given by

$$\text{NEP} = \frac{A_d^{1/2}}{D^*_\lambda} = \frac{\overline{V}_N 2\pi f^{1/2} C}{R_a} \tag{A-41}$$

or defining a new $\overline{\text{NEP}} = \text{NEP}\, f^{-1/2}$ (W/Hz) we obtain

$$\overline{\text{NEP}} = \frac{\overline{V}_N 2\pi C}{R_a} \quad . \tag{A-42}$$

For $\overline{V}_N = 1.4 \times 10^{-6}$ V, C = 8 pF and R_a = 10 A/W

$$\overline{\text{NEP}} = 7 \times 10^{-18}\ \text{W/Hz} \qquad \text{(at 19 μm)} \quad . \tag{A-43}$$

[U] Since $[D^*_\lambda]_{\text{amplifier}}$ given by Eq. (A-39) and NEP given by Eq. (A-41) are frequency dependent quantities, it is important to carefully relate f in these equations to the system bandwidth B and target image dwell time τ. Going back, Eq. (A-30) is representative of a single frequency, narrow band, determination whereas the application we are envisioning is a pulse measurement requiring a broad band system with bandwidth B = $1/2\tau$. The value of $[D^*_\lambda]_{\text{amplifier}}$ or NEP appropriate for such a measurement will be some average over the frequencies within the bandwidth B. For our purposes here we will approximate this average by using that value of $[D^*_\lambda]_{\text{amplifier}}$ or NEP corresponding to f = B/2, sort of a mid-band value.

[U] We are now in a position to determine what values of dwell time, τ, or detector area, A_d, would cause the system to become amplifier noise limited rather than say background limited. The amplifier noise limited detectivity given by Eq. (A-39) is shown in Fig. A-9 vs frequency f for a number of typical detector areas. If the background limit is assumed to be roughly

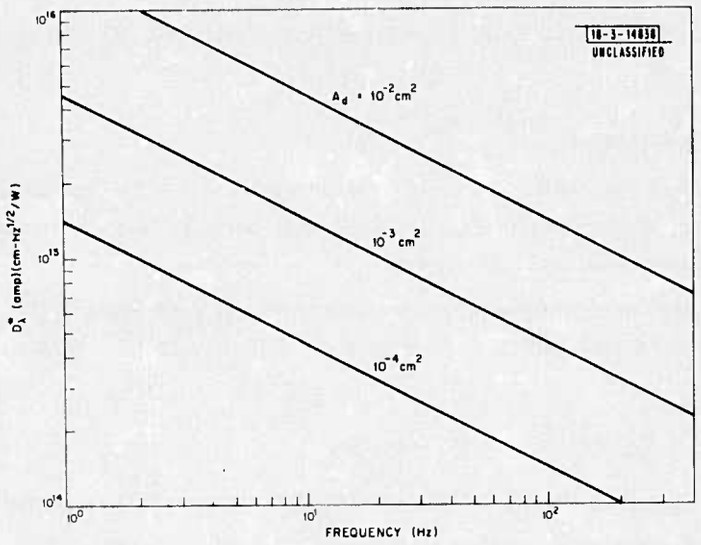

Fig. A-9. Amplifier noise limited detectivity vs frequency for various typical detector areas. [U]

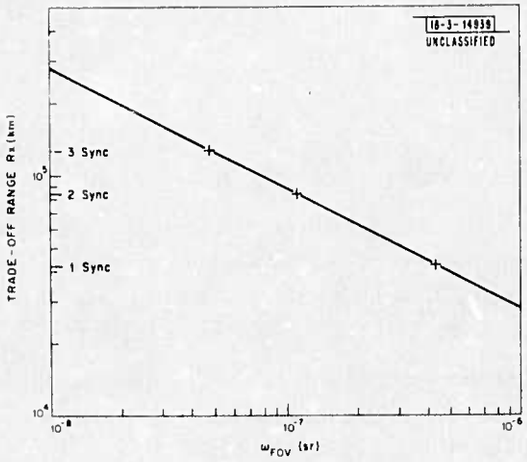

Fig. A-10. Trade-off range between amplifier noise limited and background limited operation for a scanned array vs individual detector instantaneous field-of-view. [U]

10^{15} cmHz$^{1/2}$/W, it is clear from Fig. A-9 that the system will become amplifier limited for higher frequencies (faster scan rates and lower dwell times) and smaller detectors (smaller systems and smaller fields-of-view as would be required for high star densities).

[U] At low frequencies, below a few Hz, it can also be shown that the noise in the load resistor will make a contribution. This is given by

$$V_N = (4kT_L R_L)^{1/2} \qquad (\text{Volts/Hz}^{1/2})$$

and is 4×10^{-6} V/Hz$^{1/2}$ at 15°K and about 3×10^{-6} V/Hz$^{1/2}$ at 6°K for a 2×10^{10} ohm resistor as used by Sclar. This is to be compared with an equivalent amplifier noise voltage of

$$V_N = V_N(f)\,(1 + \omega^2 R_L{}^2 C^2)^{1/2}$$

which at 1 Hz is about 2×10^{-6} V/Hz$^{1/2}$. The two become equal at about 4 Hz above which the amplifier noise dominates. Load resistor noise thus needs to be considered only for frequencies below ~4 Hz and for detector areas less than 2×10^{-4} cm^2 otherwise the detector is background limited at 10^{15} cmHz$^{1/2}$/W as assumed.

[U] The trade-off can also be considered from the viewpoint of the system range sensitivity and search rate. The range equation for a background limited system is given by Eq. (A-10b). Combining Eq. (A-34) with Eq. (A-10b) we obtain

$$R^2 = \frac{W_{\Delta\lambda} A}{4(SNR)} \frac{D}{h\nu} \left(\frac{T_o}{Q_B}\, 2n\eta\dot{\Omega}^{-1}\right)^{1/2} \quad . \qquad (A\text{-}44)$$

In the amplifier limit we obtain

$$R^2 = \frac{W_{\Delta\lambda} A}{\pi(SNR)} \frac{A_o T_o}{\overline{NEP}} \sqrt{8}\,(n\omega_{FOV}\dot{\Omega}^{-1}) \quad , \qquad (A\text{-}45)$$

using Eqs. (A-6, A-7) and $f = B/2 = 1/4\tau$. The trade-off occurs at

$$R_x^2 = \frac{W_{\Delta\lambda} A}{4\sqrt{2}\,(SNR)} \frac{\overline{NEP}}{(h\nu)} \frac{1}{W_B} \frac{\eta}{\omega_{FOV}} \qquad (A\text{-}46)$$

where we have substituted $W_B = h\nu Q_B$(W/cm^2).

[U] Assuming an $\epsilon A = 1$ m^2, 300°K target, $W_\lambda A$ at 13 μm is 26 W/μm and from the Cornell rocket data we take $W_{B,\lambda} = 3.1 \times 10^{-11}$ W/cm^2 μm (at 13 μm at 15° off ecliptic plane) so that

$$\frac{W_\lambda A}{W_{B,\lambda}} \simeq 8.26 \times 10^{11}\ \text{cm}^2 \quad .$$

Using $\overline{NEP}$ given by Eq. (A-43), $h\nu = 10^{-20}$ joules (19 μm) SNR = 7 and $\eta = 0.5$, Fig. A-10 gives the trade-off range vs ω_{FOV}. Figure A-10 indicates the range beyond which Eq. (A-44) is valid and under which Eq. (A-45) is valid. For example, if we are interested in searching only to 3X synchronous range and ω_{FOV} is less than 4.8×10^{-8} sr, then Eq. (A-45) is valid at all ranges and the system will be amplifier noise limited. If ω_{FOV} is larger than this, say 10^{-7} sr, then there

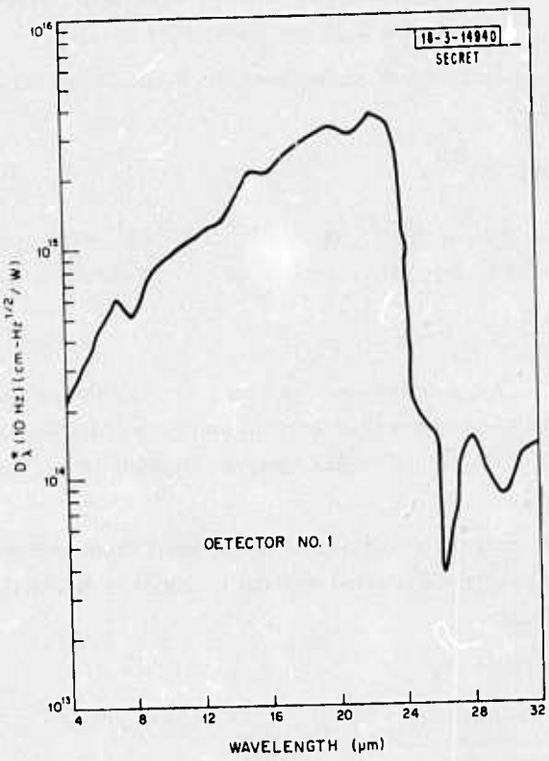

Fig. A-11. Variation of detectivity with wavelength (after Sclar). [U]

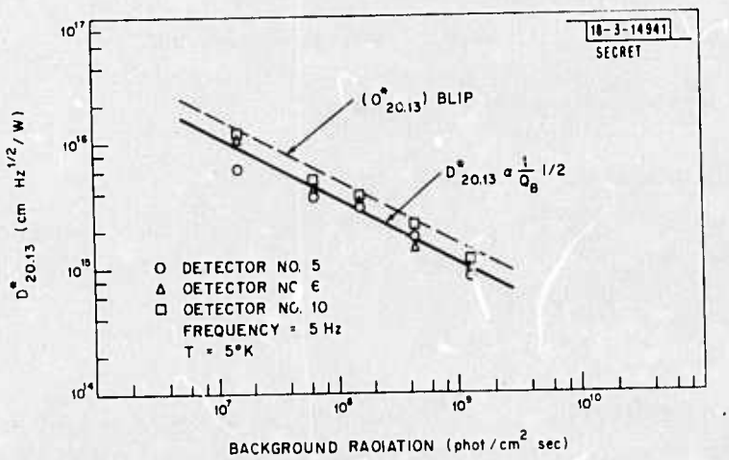

Fig. A-12. Variation of detectivity with background (after Sclar). [U]

will be a trade-off range, in this case 88,000 km, beyond which Eq. (A-44) is valid and the system becomes background limited. Again ω_{FOV} will be determined by the expected star background through Eq. (A-11).

III. STATE-OF-THE-ART

[S] The state-of-the-art regarding arrays of LWIR detectors is probably best represented by recent results obtained by Sclar for an array of 10 As doped Si detectors.[A-5] Figure A-11 shows a typical spectral detectivity curve at $Q_b = 1.5 \times 10^8$ photons/sec cm^2 at the detector plane and Fig. A-12 gives the peak detectivity vs background radiation for three of the detectors in the array. The detectivity vs detector temperature is given in Fig. A-13. A summary of results

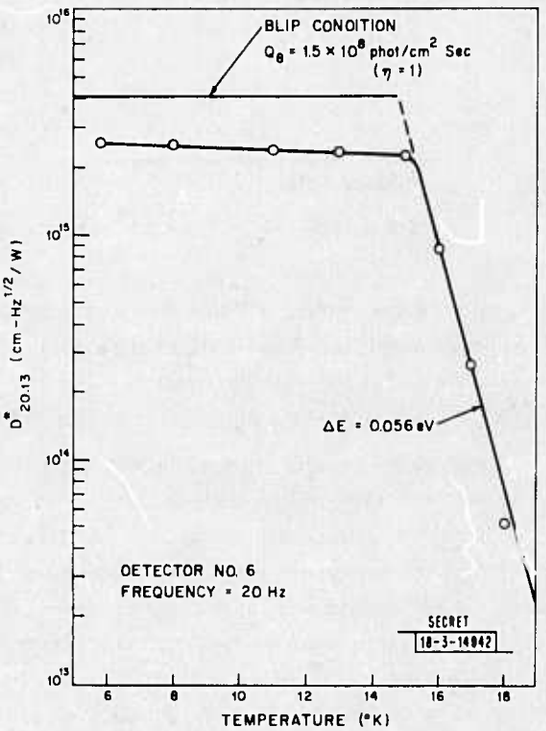

Fig. A-13. Variation of detectivity with detector temperature (after Sclar). [U]

for the array is given in Table A-4. It appears that the measurements made at 15°K and $Q_b = 1.5 \times 10^8$ photons/sec cm^2 at frequencies up to 45 Hz are detector and/or background limited. The measurements made at 5 Hz and 5°K are background limited down to 1.5×10^7 photons/sec cm^2. No high frequency measurements were made at this low temperature and low background to determine the amplifier noise limit. However, an additional set of measurements[A-6] were made on a similar array of As doped Si detectors at the Naval Electronics Laboratory Center (NELC). These measurements were made with a background of 9×10^6 photons/sec cm^2 and a detector temperature of 15° and 6°K. A summary of the 15°K results are shown in Table A-5 and typical results are shown in Fig. A-14. At low frequencies the detectivity is detector noise limited whereas at high frequencies the detectivity is amplifier noise limited. A summary of

TABLE A-4† [S]
DETECTOR PERFORMANCE‡ [U]

Detector No.	D^*_{20} (cm $Hz^{1/2}$/w)	η (%)	Frequency (Hz)	D^*_{pk} (10 Hz)
1	3.4×10^{15}	69	10	3.8×10^{15}
2	3.0	54	5, 10	3.2
3	3.5	73	5	3.3
4	3.2	61	5, 10	3.5
5	2.8	47	5	3.0
6	3.0	54	5	3.0
7	2.9	50	5, 10	3.3
8	3.2	61	10	3.4
9	2.9	50	10	3.0
10	3.7	81	5	4.0

† After Sclar.

‡ T = 15°K, $Q_b = 1.5 \times 10^8$ photons/sec cm^2.

the 6°K results are shown in Table A-6 and typical results are shown in Fig. A-15. The detectivity appears amplifier noise limited throughout the frequency range shown in Fig. A-15. The slope is close to but not exactly equal to $-1/2$ and the values closely approximate those given in Fig. A-9 for the appropriate detector area (7.6×10^{-3} cm^2).

[S] From these results it appears that modest arrays of a few dozen detectors with relatively large areas (~20 × 60 mils) can be obtained with space background limited detectivities of ~10^{15} cm$Hz^{1/2}$/W at frequencies up to f ≃ 150 Hz, τ = 1.67 msec. The only detector parameter which effects the background limited performances is the quantum efficiency, η, which is already in excess of 50 percent. Thus not much can be gained in the background limited regime except making more detectors which is significant but arduous. Because of star backgrounds and resolution requirements the space surveillance mission will require very large numbers of considerably smaller detectors. Assuming that such detectors can be made in numbers of 500-1000 and sizes ranging between 10^{-4} and 10^{-3} cm^2 they would, today, be amplifier noise limited in most situations. In this case the sensitivity depends not only on the quantum efficiency and detector gain which are already nearly optimum but also on the amplifier noise figure $V_N(f)$ and parasitic capacitance. It will be difficult to accomplish a significant reduction in parasitic capacitance although 4-5 pF would not appear as an unreasonable goal. One might hope to reduce the amplifier noise voltage significantly; however, one would thus have the noise in the load resistor to contend with. This can only be reduced by further cooling or by raising the value of R_L (noise current being proportional to R_L^{-1}). Effort is being extended in this direction but the task is not easy and order-of-magnitude improvements do not appear likely in the near future. It therefore appears reasonable to consider that an amplifier limited $\overline{NEP}$ given by Eq. (A-41) can be achieved

TABLE A-5 [C]

SUMMARY OF DATA; T = 15K, λ = 19μm, V = 6V [U]

	FREQUENCY = 5Hz			FREQUENCY = 45Hz		
Channel	Responsivity (volts/watt)	NEP (watts/$Hz^{1/2}$)	D* (cm-$Hz^{1/2}$/watt)	Responsivity (volts/watt)	NEP (watts/$Hz^{1/2}$)	D* (cm-$Hz^{1/2}$/watt)
1	4.1×10^{10}	4.1×10^{-17}	2.1×10^{15}	5.2×10^{9}	6.7×10^{-17}	1.3×10^{15}
2	3.9×10^{10}	5.4×10^{-17}	1.6×10^{15}	4.7×10^{9}	7.3×10^{-17}	1.2×10^{15}
3	3.6×10^{10}	4.4×10^{-17}	2.0×10^{15}	4.5×10^{9}	6.7×10^{-17}	1.3×10^{15}
4	3.5×10^{10}	5.1×10^{-17}	1.7×10^{15}	4.4×10^{9}	7.9×10^{-17}	1.1×10^{15}
5	5.0×10^{10}	4.0×10^{-17}	2.2×10^{15}	6.5×10^{9}	5.4×10^{-17}	1.6×10^{15}
6	4.3×10^{10}	4.6×10^{-17}	1.9×10^{15}	5.5×10^{9}	5.8×10^{-17}	1.5×10^{15}
7	5.4×10^{10}	4.4×10^{-17}	2.0×10^{15}	6.5×10^{9}	5.8×10^{-17}	1.5×10^{15}
8	4.7×10^{10}	5.8×10^{-17}	1.5×10^{15}	4.4×10^{9}	6.7×10^{-17}	1.3×10^{15}
9	3.2×10^{10}	6.2×10^{-17}	1.4×10^{15}	4.1×10^{9}	9.3×10^{-17}	0.94×10^{15}
10	2.5×10^{10}	6.7×10^{-17}	1.3×10^{15}	3.1×10^{9}	9.7×10^{-17}	0.90×10^{15}

Confidential

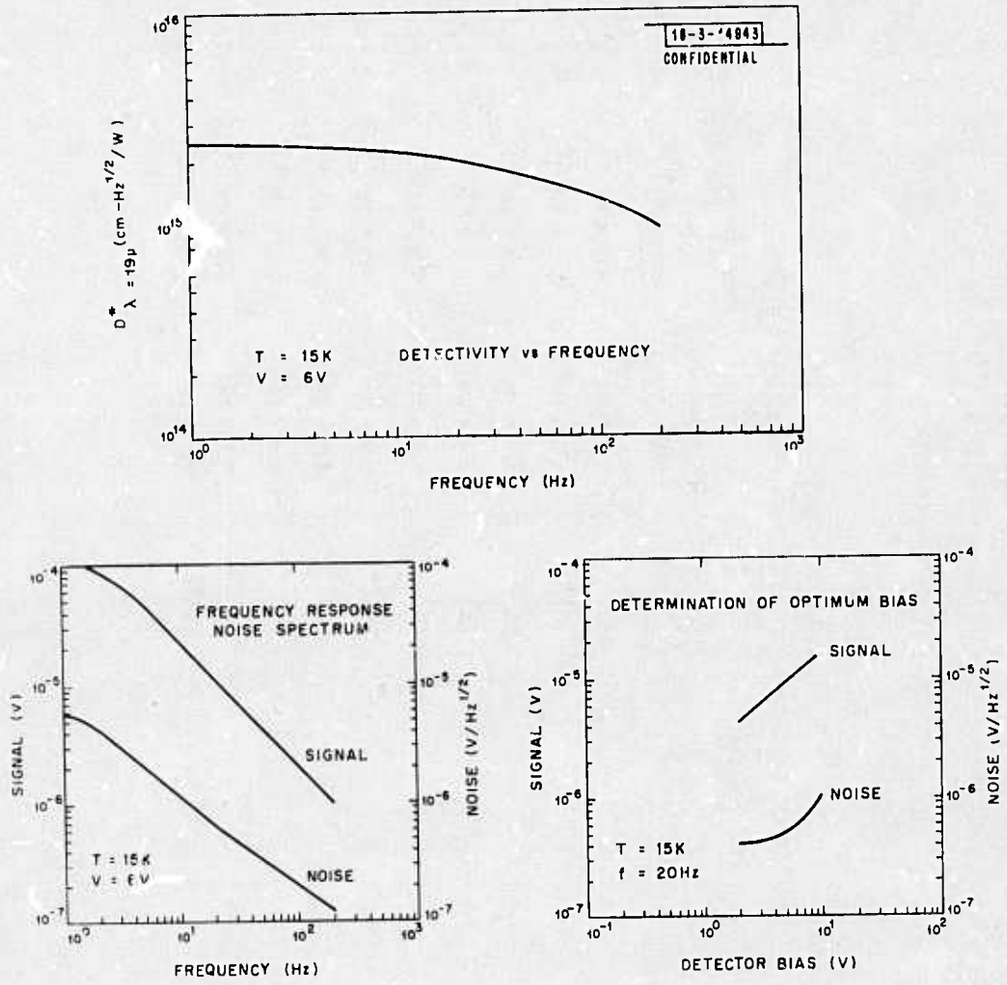

Fig. A-14. Channel 5, T = 15°K. [U]

TABLE A-6 [C]

SUMMARY OF DATA; T = 6 K, λ = 19 μm, V = 8 V [U]

	FREQUENCY = 5 Hz			FREQUENCY = 45 Hz		
Channel	Responsivity (volts/watt)	NEP (watts/$Hz^{1/2}$)	D* (cm-$Hz^{1/2}$/watt)	Responsivity (volts/watt)	NEP (watts/$Hz^{1/2}$)	D* (cm-$Hz^{1/2}$/watt)
1	5.6×10^{10}	1.4×10^{-17}	6.0×10^{15}	6.7×10^{9}	3.6×10^{-17}	2.4×10^{15}
2	5.9×10^{10}	2.2×10^{-17}	3.9×10^{15}	7.2×10^{9}	2.9×10^{-17}	3.0×10^{15}
3	5.9×10^{10}	1.2×10^{-17}	7.0×10^{15}	6.8×10^{9}	3.5×10^{-17}	2.5×10^{15}
4	5.0×10^{10}	1.6×10^{-17}	5.4×10^{15}	6.0×10^{9}	4.0×10^{-17}	2.2×10^{15}
5	6.4×10^{10}	1.3×10^{-17}	6.5×10^{15}	6.7×10^{9}	3.6×10^{-17}	2.4×10^{15}
6	4.6×10^{10}	1.4×10^{-17}	6.4×10^{15}	5.8×10^{9}	3.1×10^{-17}	2.8×10^{15}
7	6.0×10^{10}	1.3×10^{-17}	6.9×10^{15}	6.8×10^{9}	3.1×10^{-17}	2.8×10^{15}
8	5.1×10^{10}	1.4×10^{-17}	6.3×10^{15}	5.5×10^{9}	3.8×10^{-17}	2.3×10^{15}
9	4.2×10^{10}	1.6×10^{-17}	5.5×10^{15}	5.0×10^{9}	4.6×10^{-17}	1.9×10^{15}
10	4.6×10^{10}	1.4×10^{-17}	6.4×10^{15}	5.8×10^{9}	4.0×10^{-17}	2.2×10^{15}

Confidential

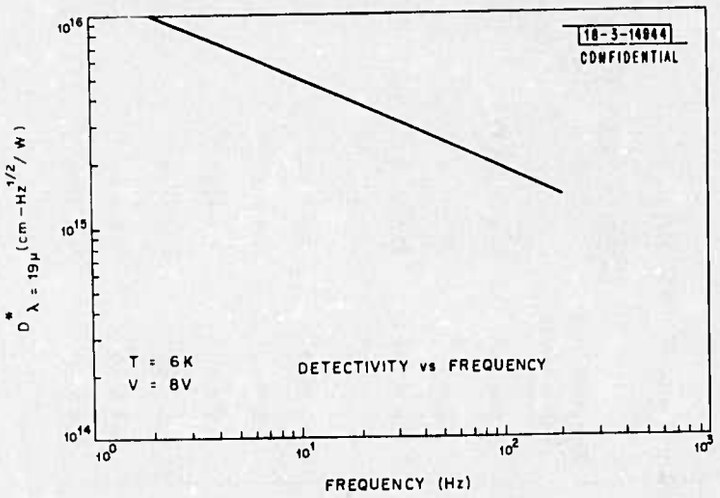

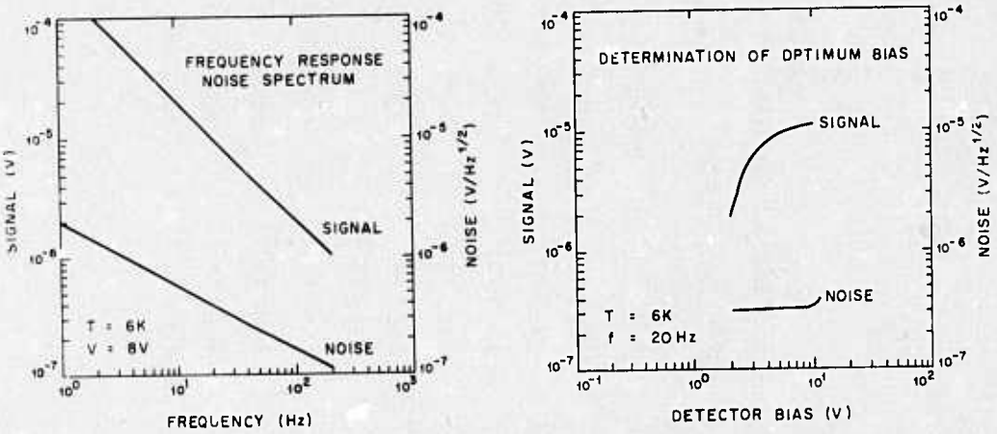

Fig. A-15. Channel 5, T = 6°K. [U]

for a linear array of detectors and that the trade-off between background and amplifier limited performance will be given by Eqs. (A-44 thru A-46) and as represented in Fig. A-10.

IV. EXOATMOSPHERIC SENSOR CAPABILITIES

[S] In order to obtain an estimate of what values of NEFD could reasonably be achieved we consider the performance specifications of two infrared sensors which already have been operated exoatmospherically, CMP (Celestial Mapping Program)[A-7] and Hi-Star;[A-8] one which is under construction, Hi-Hi-Star;[A-9] and two which are under consideration for the future, MTS (Midcourse Tracking Satellite)[A-10] and MSS (Midcourse Surveillance System).[A-11] The performance specifications for these sensors are given in Table A-7.

[S] The CMP satellite was launched successfully on 17 October 1971 and employed a two-stage, closed-cycle VM refrigerator designed to cool the telescope to 55°K under 1.5 W earth radiation loading. The sensor was a modified AFIRST (advanced far infrared search-track). It is clear that the values of NEP and D* obtained are significantly worse than those obtained by the Hi-Star sensor. The difference probably lies in the poorer cooling of the telescope. From Fig. A-6 and Table A-7 we would estimate that the telescope temperature is probably higher than 55°K and is probably close to 65°K. In order to correct this situation one would have to employ a three-stage cooler.

[S] The Hi-Star sensor has been flown on an Aerobee 350 rocket probe to an altitude of 200 miles. The factor of ~2.5 degradation in NEFD for flight operation may be due to scattered earth radiation. The Hi-Hi-Star sensor is currently under construction and is designed to be operated first on a probe using liquid helium reservoir for cooling and finally on a satellite using a closed cycle refrigerator. The MTS and MSS system concepts were developed specifically for BMD.

[S] Consider what values of NEFD are required for the satellite detection task. For this we will assume a $1\,m^2$, unit emissivity target at a range of 127,000 km (3× Synchronous). This yields the following:

	$W_{\Delta\lambda}A$ (W)	W (W/cm^2)	NEFD (W/cm^2)
3-5 μm	5.6	1.1×10^{-20}	1.6×10^{-21}
8-14 μm	173	3.4×10^{-19}	4.9×10^{-20}
16-22 μm	81	1.6×10^{-19}	2.3×10^{-20}

assuming a required SNR of 7. Thus for the two longer wavelength regions we require an NEFD of $2\text{-}5 \times 10^{-20}\,W/cm^2$, a factor of 10^3 better than Hi-Star and a factor of 20 to 50 better than the predicted sensitivity of Hi-Hi-Star.

[U] According to Fig. A-12, the sensor searching at 3× synchronous range will be marginally background limited for $\omega_{FOV} = 10^{-7}$ sr and we can use Eq. (A-44) to determine the optics diameter and number of detector elements necessary to scan at the rate $\dot{\Omega}$. Using

TABLE A-7 [S]

SENSOR COMPARISON [U]

	CMP (Ref. A-7)	Hi-Star (Ref. A-8)	Hi-Hi-Star (Ref. A-9)	MTS (Ref. A-10)	MSS (Ref. A-11)
OPTICS					
Aperture (inches)	6.5	6.5	14	10	10
f number	3.16	3.16	2.18	2.7	2.7
Total Inst FOV (deg×mr)	1.3 × 0.75	1.2 × 1	2.5 × 0.5	15 × 0.25	15 × 0.21
Efficiency (T_o)	0.6	0.45	0.5	0.3-0.5	0.5
Temperature (°K)	55	<40	<40	<35	<35
DETECTOR					
Material	Ge:Hg, Ge:Cu	Ge:Hg, Ge:Cu	Si:As (g)	Si:As	Si:As (g)
Size (inches)	0.015 × 0.074	0.020 × 0.062	0.015 × 0.075	0.0067 × 0.0185	0.0057 × 0.016 (g)
Resolution (mr)	0.75 × 3.6	~1 × 3	~0.5 × 2.5	0.25 × 0.69	0.21 × 0.59 (g)
Detectors/channel	7	8	18	555	650
Channels (μm)	8-14, 16-22	3-5, 8-14, 16-22	3-5, 8-14, 16-22	5.5-10, 16-22	8-12
Temperature (°K)	15	4.6-13	4.6-13	15	15 (g)
NEP ($W/Hz^{1/2}$)	$2.9\text{-}4.3 \times 10^{-15}$	3.2×10^{-16} (c)	1.3×10^{-16} (e)	$10,6 \times 10^{-17}$ (e)	5×10^{-17} (e)
D* ($cmHz^{1/2}/W$)	$2\text{-}3 \times 10^{14}$	2.8×10^{14} (c)	6.5×10^{14} (e)	$3,5 \times 10^{14}$ (e)	5×10^{14} (e)
SYSTEM					
Dwell Time (msec)	6.3	1.5	29	0.8	1.7
NEFD (W/cm^2)	$2\text{-}3 \times 10^{-16}$ (a)	~6×10^{-17} (c)	1.1×10^{-18} (e)	10^{-17}	3.4×10^{-18} (e)
	$8\text{-}11 \times 10^{-16}$ (b)	~1.5×10^{-16} (d)			
Weight (lbs)	32	35	150	250 (f)	(g)

(a) 8-14 μm flight (c) lab average (e) predicted (g) not specified
(b) 16-22 μm flight (d) flight average (f) total system

Secret

$$W_{\Delta\lambda}A = 173\,W\ (8\text{-}14\,\mu m)$$

$$W_B = 2.1 \times 10^{-10}\ W/cm^2$$

$$h\nu = 1.85 \times 10^{-20}\ \text{joules}\ (10.7\,\mu m, \text{appropriate midband value})$$

$$T_o = 0.5$$

$$\eta = 0.5$$

$$SNR = 7$$

$$R = 1.25 \times 10^{10}\ cm\ (3\times\ \text{synchronous})$$

we obtain from Eq. (A-44)

$$\dot{\Omega}^{1/2} = 8.5 \times 10^{-4} n^{1/2} D\ (sr/hour)\ (D\ in\ cm) \quad .$$

Using

$$n = 500$$

$$D = 28" = 71\,cm \quad ;$$

we obtain

$$\dot{\Omega} = 1.8\,sr/hour \quad .$$

The characteristics of this sensor are given in Table A-8.

[U] Note that the wavelength range can be extended to increase the scan rate for the same system as indicated in Table A-9. Of course additional cooling would be required for the longer wavelength systems.

V. POSSIBLE IR VIDICON SENSOR CAPABILITIES

[S] As a possible alternative to an IR sensor consisting of a large number of individual photoconductive elements consider an IR Vidicon consisting of a quasi continuous photoconductive layer with readout provided by a scanning electron beam. A schematic diagram of a return-beam-vidicon (RBV) employing an offset cathode is shown in Fig. A-16.[A-12] The structure is shown employing a Ge:Cu[11] photoconductive sensing layer and liquid nitrogen cooling. For our purposes we would propose using Si:As or Si:B for the sensing layer and cooling the entire housing to about 10° – 15°K. This should provide LWIR sensitivity out to 24 μm.

[U] The advantage of using an IR Vidicon in place of a linear array comes in the large increase in the number of effective individual sensing elements which can be realized. It should be possible to fabricate a silicon vidicon retina with a useful area of up to $25\,cm^2$ (~2" × 2") and a minimum resolution element size of about 50 μm giving a total number of 10^6 effective resolution elements. This is an increase by a factor of approximately 2000 over the more ambitious linear arrays discussed above. If all else were the same this would translate into an increase in scan rate by a factor of 2000 or in range by a factor of $(2000)^{0.25} = 6.7$.

TABLE A-8 [S]

SENSOR SPECIFICATIONS [U]

OPTICS	
Aperture (inches)	28
f-number	2
Total Inst. FOV	143° × 0.2 mr
Efficiency (T_o)	0.5
Temperature (°K)	< 45
DETECTOR	
Material	Si:As
Size (inches)	0.011 × 0.028
Resolution (mr)	0.2 × 0.5
Detectors/row	500
Number of rows (a)	2
Wavelength (μm)	8-14
Temperature (°K)	15
NEP ($W/Hz^{1/2}$) (b)	4×10^{-17}
D* ($cmHz^{1/2}/W$) (b)	10^{15}
SYSTEM	
Dwell time (sec)	0.1 (c)
NEFD (W/cm^2) (b)	5×10^{-20} (c)
Scan rate (sr/hour)	1.83 (c)

(a) Two rows of detectors are indicated in order to facilitate discrimination between satellite targets and stars as discussed in Appendix C.

(b) The D*, NEP and NEFD numbers quoted are the appropriate values for the in-hand wavelength of 10.7 μm and an f = 2 system.

(c) At R = 3 times synchronous.

TABLE A-9 [U]

SCAN RATE VS SPECTRAL WAVELENGTH RANGE [U]

Spectral Range (μm)	H (W)	W_B (W/cm^2)	$\dot{\Omega}$ (sr/hour)
8-14	173	2.10×10^{-10}	1.8
6-14	210	2.54×10^{-10}	2.2
6-18	295	3.57×10^{-10}	3.3
6-24	360	4.35×10^{-10}	4.8

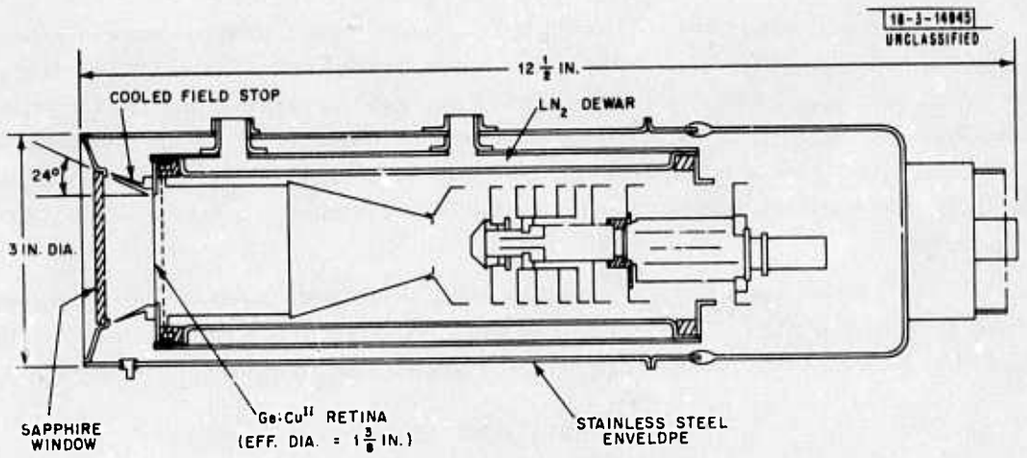

Fig. A-16. Z-7934 copper-doped germanium IR vidicon. [U]

[U] The vidicon sensitivity can be expressed in a manner formally identical to that of the linear array.

$$R^2 = \frac{W_{\Delta\lambda} A}{\pi(SNR)} \frac{A_o T_o}{NEP} (2n\omega_{FOV})^{1/2} \left(\frac{t_F}{\Omega_{FOV}}\right)^{1/2} \tag{A-47}$$

where now NEP is the noise-equivalent-power for the vidicon, n is the total number of vidicon resolution elements, t_F is the vidicon frame time, Ω_{FOV} is the total instantaneous vidicon field-of-view and

$$\omega_{FOV} = A_e/F^2 \tag{A-48}$$

where A_e is the vidicon resolution element area and F is the system focal length. In general A_e/F^2 will be sufficiently small to avoid the star background problem which was a limiting factor for the linear array. Note that Eq. (A-48) can be rewritten in terms of the total vidicon retina area $A_r = nA_e$,

$$R^2 = \frac{W_{\Delta\lambda} A}{\pi(SNR)} \frac{A_o T_o}{NEP} \frac{(2A_r)^{1/2}}{F} \left(\frac{t_F}{\Omega_{FOV}}\right)^{1/2} . \tag{A-49}$$

The system sensitivity thus hinges critically on the realizable vidicon NEP. In the present application this will be given by

$$NEP = (2qA_e W_b / R_a m)^{1/2} \tag{A-50}$$

where

W_b = vidicon retina irradiance due to the background

A_e = resolution element area

R_a = retina responsivity

m = vidicon modulation index .

If Eq. (A-50) applies the system is background limited.

[U] The above analysis is applicable for a return-beam-vidicon (RBV) readout in which the entire return beam is collected and amplified or for an Isocon readout, in which only that portion of the return beam which has physically interacted with and has been scattered by the vidicon retina surface is collected. The intensity of this scattered beam is directly proportional to the signal intensity and there is no excess beam current to contribute to the shot noise as in the case of the RBV. The effective modulation index for the Isocon readout is about 0.5 compared to about 0.1 for the RBV.

[S] An LWIR return beam vidicon tube employing a Ge:Zn^{II} retina has been developed and tested by General Electric.[A-13] The results of their evaluation of this tube are indicated in Table A-10. Also shown in the table are the projected performance characteristics of an LWIR

TABLE A-10 [S]
VIDICON CHARACTERISTICS [U]

RETINA MATERIAL	Measured RBV Ge:Zn^{II}	Projected RBV Si:B	Projected Isocon Si:B	Advanced Isocon Si:B
RETINA AREA, A_r (cm^2)	5	25	25	25
RESOLUTION AREA, A_e (cm^2)	5×10^{-5}	2.5×10^{-5}	2.5×10^{-5}	2.5×10^{-5}
NUMBER OF ELEMENTS, n	10^5	10^6	10^6	10^6
RESPONSIVITY, R_a (A/W)	0.02	0.4	0.4	2.5
MODULATION INDEX, m	0.1	0.1	0.5	0.5
DYNAMIC RANGE, Dy	50	10	>100	>100
BACKGROUND, W_b (W/cm^2)	10^{-5}	1.2×10^{-11}†	1.2×10^{-11}†	1.2×10^{-11}†
NEP ($W/Hz^{1/2}$)	7×10^{-13}	4.8×10^{-17}	2.2×10^{-17}	8.6×10^{-18}

† 8-14 μm, ±15° off ecliptic, f = 1.5, T_o = 0.5

return-beam vidicon and an LWIR Isocon as well as those of an advanced Isocon. The primary differences between the three postulated vidicons and measured performance of the Ge:Zn^{II} General Electric vidicon are:

(a) Larger retina area, 2 × 2 inches (3-inch Si wafers)
(b) Somewhat improved resolution
(c) Increased responsivity (more heavily doped Si)
(d) Greatly reduced background corresponding to space operation.

The first two of these factors result in the ten-fold increase in the number of resolution elements. The responsivity is given by

$$R_a = q\eta G/h\nu \qquad \text{(A-51)}$$

where η and G are the vidicon retina quantum efficiency and gain respectively and $h\nu$ is the photon energy. For the Ge:Zn^{II} retina $\eta G = 2.3 \times 10^{-3}$ (10.6 μm) whereas the projected ηG product

for the doped Si retina at 12.4 μm is 4×10^{-2} (η = 0.2 and G = 0.2) corresponding to a greater absorption coefficient. The ηG product for the advanced Isocon was assumed to be 0.25 (η = 0.5, G = 0.5) which is probably the maximum that one could reasonably consider for vidicon operation.

[U] There is an operational problem encountered when one attempts to use a vidicon in a search scheme or in a scanning mode. This arises from the fact that the vidicon employs a signal integration process in order to achieve high sensitivity. One way to accomplish this is to step scan the telescope allowing the image to be integrated by the vidicon. After a sufficient period the image could be read out, the telescope stepped to the next position, the remaining image on the vidicon erased and the process repeated. In this process we might envision that the readout occurs in one tenth the total frame time and that the integration occurs over most of this.

[U] There are two additional considerations which must be taken into account in estimating the projected and advanced vidicon performance characteristics. The first is the discharge of the vidicon retina due to the background radiation. The rate at which the voltage across the retina changes is given by

$$\frac{dv}{dt} = \frac{i_b}{C} \tag{A-52}$$

where C is the retina capacitance given by

$$C = \frac{A_r \epsilon}{d} \tag{A-53}$$

where ϵ is the retina dielectric constant and d is the retina thickness. Using $i_b = R_a A_r W_b$ this gives

$$\frac{dv}{dt} = \frac{R W_b d}{\epsilon} \tag{A-54}$$

where W_b is the background irradiance at the retina. Typical charging voltages are 6 V for d = 100 μm.

[U] Using $W_b = 1.2 \times 10^{-11}$ W/cm^2, $\epsilon = 10^{-12}$ F/cm, appropriate for Si, and limiting ΔV to 1 volt we obtain a limitation of

$$R_a t_F \leqslant 8.5 \text{ amp sec/watt} \quad .$$

[U] This limitation, however, can be circumvented, in principle, where necessary by reading out and recharging the retina several times and using an electron storage tube to integrate the signal over several frames. Assuming no signal-to-noise degradation due to the storage tube this results in the same range-sensitivity equation with t_F becoming the total integration time.

[U] The second, and more fundamental, consideration is the limitation imposed by the motion of the target. This limits the length of time over which we can obtain integration of the target

signal in a single resolution cell. Substituting Eq. (A-50) in Eq. (A-47) and using Eq. (A-33), we obtain for the background limited range sensitivity of the vidicon

$$R^2 = \frac{W_{\Delta\lambda} A}{2(SNR)} D\left(\frac{T_o n R_a m}{q W_B}\right)^{1/2} \left(\frac{t_F}{\Omega_{FOV}}\right)^{1/2} . \quad (A-55)$$

The limitation on the frame time due to the target motion is given by

$$t_F \leq \frac{(A_e)^{1/2}}{\alpha F} \quad (A-56)$$

where α is the angular rate of target motion in radians/sec. The total vidicon instantaneous field-of-view is given by

$$\Omega_{FOV} = \frac{A_r}{F^2} = \frac{n A_e}{F^2} . \quad (A-57)$$

Substituting Eq. (A-56) and (A-57) in Eq. (A-55), we obtain

$$R^2 = \frac{H}{2(SNR)} D\left(\frac{T_o R_a m F}{q W_B \alpha (A_e)^{1/2}}\right)^{1/2} \quad (A-58)$$

and for the angular search rate,

$$\dot{\Omega} = \frac{\Omega_{FOV}}{t_F} = \frac{\alpha A_r}{F(A_e)^{1/2}} . \quad (A-59)$$

[U] It is possible using Eqs. (A-54) and (A-56) along with

$$W_b = \frac{T_o W_B}{4f^2} \quad (A-60)$$

to determine if the frame time is limited by target motion or retina discharge. The retina discharge frame time limit is given by

$$t_F \leq \frac{4f^2 \epsilon \Delta V}{R_a T_o W_B d} . \quad (A-61)$$

We assume a value of $\alpha = 15\,\mu$ rad/sec, corresponding to the angular motion of a satellite in synchronous orbit, and

$$W_{\Delta\lambda} A = 173\,W$$

$$R = 1.25 \times 10^{10}\,cm$$

$$SNR = 7$$

$$W_B = 2.1 \times 10^{-10}\,W/cm^2$$

$$T_o = 0.5$$

$d = 100\,\mu m$

$\epsilon = 10^{-12}\,F/cm$

$\Delta V = 1$ volt

$f = 1.5$

$A_e = 2.5 \times 10^{-5}\,cm^2$.

Table A-11 gives the results for the three Si:B vidicons characterized in Table A-10. All three sensors are designed to give an NEFD of $5 \times 10^{-20}\,W/cm^2$ so that they are capable of detecting a $1\,m^2$, 300°K, $\epsilon = 1$ target at 125,000 km range with a signal-to-noise ratio of 7. For purposes of this study we will consider a projected Isocon sensor with the characteristics given in Table A-12. The sensor described in Table A-12 has somewhat more than adequate sensitivity to detect a $1\,m^2$, 300°K, $\epsilon = 1$ target at 125,000 km with SNR = 7 while scanning at a rate of almost 12 sr/hour.

TABLE A-11 [S]
VIDICON SENSOR CHARACTERISTICS [U]

	Projected RBV	Projected Isocon	Advanced Isocon
RETINA AREA, A_r (cm^2)	25	25	25
RESOLUTION AREA, A_e (cm^2)	2.5×10^{-5}	2.5×10^{-5}	2.5×10^{-5}
NUMBER OF ELEMENTS, n	10^6	10^6	10^6
RESPONSIVITY, R_a (A/W)	0.4	0.4	2.5
MODULATION INDEX	0.1	0.5	0.5
NEP ($W/Hz^{1/2}$)	4.8×10^{-17}	2.2×10^{-17}	8.6×10^{-18}
OPTICS DIAMETER, D (cm) REQUIRED MINIMUM	23.8	13.9	12.9
f-NUMBER	1.5	1.5	1.5
FRAME TIME, t_F (sec)	9.3	16.0	3.4
FIELD-OF-VIEW, $\Omega_{FOV}^{1/2}$ (rad)	0.14	0.24	0.26
NEFD (W/cm^2)	5×10^{-20}	5×10^{-20}	5×10^{-20}
SCAN RATE, $\dot{\Omega}$ (sr/hour)	7.6	13	71
LIMITATION	Target motion	Target motion	Retina Discharge

TABLE A-12 [S]

PROJECTED ISOCON SENSOR CHARACTERISTICS [U]

RETINA MATERIAL	Si:B
RETINA AREA (cm^2)	25
RESOLUTION AREA (cm^2)	2.5×10^{-5}
NUMBER OF ELEMENTS	10^6
RESPONSIVITY (A/W)	0.4
MODULATION INDEX	0.5
FRAME TIME (sec)	12.5
BANDWIDTH (Hz)	0.04
DYNAMIC RANGE	>100
BACKGROUND (W/cm^2)†	1.2×10^{-11}
NEP ($W/Hz^{1/2}$)	2.2×10^{-17}
OPTICS DIAMETER (cm)	16.5 (6.5")
OPTICS TRANSMISSION	0.5
OPTICS TEMPERATURE (°K)	<45
DETECTOR TEMPERATURE (°K)	≤10
WAVELENGTH RANGE (μm)	8-14
FIELD-OF-VIEW (rad)	0.2
NEFD (W/cm^2)	4×10^{-20}
SCAN RATE‡ (sr/hour)	11.75

† 8-14μm, ±15° off ecliptic, f = 1.5, T_o = 0.5, at retina

‡ +1 m^2, 300°K, ϵ = 1 target at 125,000 km range at SNR = 9

REFERENCES

A-1. See for example, P.W. Kruse, L. D. McGlauchlin and R.B. McQuistan, Elements of Infrared Technology (John Wiley & Sons, 1962), UNCLASSIFIED.

A-2. R. J. Keyes and T. M. Quist, "Low Level Coherent and Incoherent Detection in the Infrared," Semiconductors and Semimetals Vol. 5 (Academic Press, 1970), UNCLASSIFIED.

A-3. J. S. Garing, A. J. Stair, Jr. and R. W. Walker, "Long Wavelength Infrared Backgrounds" [U], J. Defense Research 1A, 85 (1969), SECRET, RESTRICTED DATA.

A-4. B. T. Soifer, J. R. Houck and M. Harwit, "Rocket-Infrared Observations of the Interplanetary Medium," Astrophys. J. 168, L73 (1971), UNCLASSIFIED.

A-5. N. Sclar, "Detector Array Development, Final Technical Report" [U], Contract No. DAHC60-71-C-0023 ARPA Order No. 1292, North American Rockwell Electronics Group, 23 December 1971, SECRET.

A-6. "Properties of Photodetectors" [U] (Photodetector Series, 87th Report, "Evaluation of a 10-Element, Arsenic-Doped Silicon Array [U]") Naval Electronics Laboratory Center, Electronic Materials Sciences Division, 15 February 1972, CONFIDENTIAL.

A-7. Final Report, Celestial Mapping Program (CMP), Contract F04701-70-C-0064, Report No. P71-478, Hughes Aircraft Co., Culver City, California, December 1971, SECRET.

A-8. J. H. Oakley, "Hi-Star System Description" [U], Proc. 9th Midcourse Measurements Meeting, p. 307, SECRET.

A-9. R. G. Walker, private communication, UNCLASSIFIED.

A-10. Indian Summer Integration Study Final Report, National Value Defense Volume IV, Sensors and Discrimination Boeing Co., Seattle, Washington (ABMDA Contract DAHC-04-71-C-0003) D180-10595-5 (March 1971), SECRET, RESTRICTED DATA.

A-11. Technical Report, Midcourse Surveillance System Study, Final Report, System Analysis SAMSO-TR-70-190, May 1970, Philco-Ford Corp, Newport Beach, California (Contract F04701-69-C-0400), SECRET, RESTRICTED DATA.

A-12. Reticulated Copper-Doped Germanium IR Vidicon Program Special Technical Report, 15 February 1971, AD 514283 prepared by General Electric for ABMDA under Contract DAHC 60-70-C-0099, ARPA Order No. 1292, SECRET.

A-13. R. L. Gulatsi and F. M. Leccese, Vidicon Development Program 11th Midcourse Measurements Meeting, p. 183, SECRET.

(This page is unclassified)

UNCLASSIFIED

Security Classification

DOCUMENT CONTROL DATA – R&D

(Security classification of title, body of abstract and indexing annotation must be entered when the overall report is classified)

1. ORIGINATING ACTIVITY *(Corporate author)* Lincoln Laboratory, M.I.T.	2a. REPORT SECURITY CLASSIFICATION SECRET 2b. GROUP XGDS-3

3. REPORT TITLE

Sensor Capabilities (Title UNCLASSIFIED)

4. DESCRIPTIVE NOTES *(Type of report and inclusive dates)*

Technical Note

5. AUTHOR(S) *(Last name, first name, initial)*

Dimmock, John O.

6. REPORT DATE 18 January 1974	7a. TOTAL NO. OF PAGES 40	7b. NO. OF REFS 13
8a. CONTRACT OR GRANT NO. F19628-73-C-0002 b. PROJECT NO. ARPA Order 600 c. d.	9a. ORIGINATOR'S REPORT NUMBER(S) Technical Note 1974-6 9b. OTHER REPORT NO(S) *(Any other numbers that may be assigned this report)* ESD-TR-74-13	

10. AVAILABILITY/LIMITATION NOTICES

None

11. SUPPLEMENTARY NOTES None	12. SPONSORING MILITARY ACTIVITY Advanced Research Projects Agency, Department of Defense

13. ABSTRACT

[U] This note describes the detailed calculations and considerations necessary to estimate infrared exoatmospheric sensor capabilities. Two types of sensors are compared, an infrared vidicon type image tube and a scanned linear array. Although both systems appear capable of high-altitude satellite surveillance, the required optics diameter for the vidicon system is significantly less than for the linear array.

14. KEY WORDS

sensors
satellite surveillance
vidicon system
linear array

UNCLASSIFIED

Security Classification

(This page is unclassified)